Study on Interaction Mechanism of Segment in Stratum of TBM Construction Overpass Building

Dapeng Liu , Ke Wu * , Wenbin XU , Zhongyu DOU , Zhenhua LIU , Jie SUN

Posted Date: 19 July 2023

doi: 10.20944/preprints202307.1312.v1

Keywords: subway tunnel; formation deformation; numerical simulation; impact analysis; TBM

Article

Study on Interaction Mechanism of Segment in Stratum of TBM Construction Overpass Building

Dapeng Liu, Ke Wu *, Wenbin Xu, Zhongyu Dou, Zhenhua Liu and Jie Sun

School of Civil Engineering, Shandong University, Jinan 250061, China
* Correspondence: wuke@sdu.edu.cn

Abstract: To solve the problem of deformation and stress in segments when a full-face hard rock tunnel boring machine (TBM) tunnel for an urban subway passes through existing buildings, a three-dimensional mechanical calculation model of TBM tunneling under existing buildings was established based on numerical analysis to comprehensively study the spatial attributes of tunnel segments during TBM tunneling. The Qingdao Metro Line 1 TBM tunnel in the hard rock stratum of Xiaobei District passes through existing buildings. The results indicated that (1) the stress and deformation of the segments were different at different positions. The horizontal and vertical stress and displacement of the segments in front of the building were significantly affected by the building. When the segment was not in the area below the horizontal plane of the building, the vertical stress of the segment was significantly greater than the two stresses in the horizontal direction. (2) The vertical displacements of the vault and the arch bottom were the largest, and the influence of vertical accessories was stronger when the segment was closer to the building.(3) When the tunnel was excavated to approximately one tunnel diameter in front of the building, the building was affected. If the surrounding rock is unstable, the excavation face may collapse and the ground surface may sink, possibly leading to inclination, cracking, and uneven settlement of the building.

Keywords: subway tunnel; formation deformation; numerical simulation; impact analysis; TBM

1. Introduction

The load on the upper part of a segment increases during excavation of an underground rail transit tunnel, and the original equilibrium state of the soil changes. The planned route of rail transit often passes through busy urban areas with a dense population, heavy traffic, and forest buildings, and is inevitably affected by buildings and surrounding rock soil. When the soil settlement reaches a certain point, it can have an irreparable effect on the safe use of surface buildings (structures). When tunnel construction crosses an existing road, if the stratum settlement is not effectively controlled, the road surface sinks and collapses, causing accidents and traffic paralysis. Stratum deformation caused by excavation is indirectly intensified by the upper load and transmitted to the segment through the surrounding rock of the formation. Carelessness in the construction process threatens the safety of construction personnel, urban residents, and property. Formation deformation is a direct cause of destruction of surface roads and structures in an underpass project. At present, commonly used tunnel excavation methods include new Austrian tunneling, shield tunneling, and shallow buried and concealed excavation; however, regardless of the method, the original equilibrium state is inevitably destroyed, producing a secondary stress field from the change in surrounding rock stress, resulting in consolidation deformation of soil and surface settlement. Geological conditions, supporting measures, construction technology, and tunnel section shape affect the settlement mode and amount of settlement; reasonable prediction of surface settlement can effectively guide construction and optimize the design.

Researchers have extensively studied the ground deformation law of segments in subway tunnel construction. The influencing factors of foundation reaction, apparent shear modulus of foundation, apparent stiffness of support, and interaction curves have been studied [1]. The effects of the in situ

stress ratio on the stress path, stress cracking, and GRC of the tunnel arch were studied through numerical analysis, and the effectiveness of the program was verified. The deformation law and mechanism of a new subway tunnel passing through existing objects were studied; comprehensively analyzed effective control measures, optimized construction methods, and support measures were proposed [2–3]. The failure modes of the excavation face of a single tunnel and an existing tunnel were studied using a transparent soil model test and numerical simulation [4]. It was found that the failure mode of the single tunnel was spherical failure due to soil arching; the failure mode of crossing the existing tunnel was wedge failure. The surface settlement of the crossing of the existing tunnel was noticeably reduced, indicating that the existing tunnel weakened surface settlement. An innovative simulation technology was developed, combining the computational efficiency of detailed process-oriented finite element (FE) simulations (sub-model) and element models (surrogate model) [5]. The simulation results demonstrated that the proposed hybrid modeling method was effective. The influence of the transverse range of the tunnel section on tunnel convergence was studied using finite difference software FLAC (3D) [6]. On this basis, a synthesis function was proposed to produce the minimum cross-sectional area within a given error range. After simulating several types of rocks, a general model with a minimum cross-sectional area was proposed. An analytical method was proposed to study the response of existing tunnels to new tunnel excavation [7]. With little research on the influence of foundation pit excavation on existing double-track tunnels below, 26 domestic engineering examples of foundation pit excavation and unloading of subway tunnels were analyzed. A modified empirical formula for the maximum uplift value was proposed for double-track tunnels in a soft soil area; the relationship between the maximum uplift value and the unloading rate of double-track tunnels with different skew widths was proposed. Based on the Beiheng tunnel project, the influence of viaduct box culvert foundation pit construction on the hyperbolic Metro Tunnel of Shanghai Metro Line 13 was analyzed, the influence law for different excavation methods on the double-track tunnel was discussed, the maximum uplift value for the double-track tunnel based on the proposed modified empirical formula was predicted, and construction suggestions for tunnel deformation control were presented. A three-dimensional numerical analysis model of a shield tunnel segment reinforced with a steel plate was established using the finite element numerical simulation method [9]. On this basis, a numerical simulation test of a segment reinforced with a steel plate was designed and conducted. The stress distribution law of the connection interface between the steel plate and the segment was analyzed when the joint staggered, and the force transfer mechanism between the steel plate and the segment was determined; guiding suggestions for the reinforcement of shield tunnels were proposed. Based on the displacement control Schwarz alternating method and the theory of complex function, and the elliptic convergence deformation boundary condition around the tunnel, a calculation method for the surrounding strata deformation caused by excavation of a double-line shield tunnel with an arbitrary layout was proposed [10].

This study focuses on the segment stress deformation and stratum deformation in TBM tunnel construction undercrossing urban buildings. A single tunnel undercrossing a single building was established as the model. The stress displacement deformation at different positions of the vault, arch waist, and arch bottom were analyzed for different groups of segments, and the stratum deformation and settlement were analyzed with different tunneling progress.

2. Numerical calculation models and methods

2.1. Project overview

The Xiaocun Station-Nanling Station section line runs north along Renmin Road to the intersection of Renmin Road and Ruichang Road. The current width of Renmin Road is approximately 20 m; the planned road width is 40 m. The interval line was mainly located below Renmin Road; there were a large number of old residential buildings and shops on both sides of the road, approximately 1-9 floors high. Renmin Road is an urban trunk road with ground vehicles and heavy traffic. A large number of heat, power, gas, mail, telecommunications, cable TV, sewage,

Preprints (www.preprints.org) | NOT PEER-REVIEWED | Posted: 19 July 2023 doi:10.20944/preprints202307.1312.v1

rainwater, tap water, and other pipelines are buried at a depth of 1-3 m; the tunnel depth is approximately 25-36 m. The area is a denuded hilly landform with slight fluctuation and an elevation of 26-36 m. The construction section of the TBM interval was 964.25 m (mileage: ZSK40 + 795.550–ZSK41 + 759.800), right line 960.798 m (mileage: YSK40 + 795.550–YSK41 + 756.348), extending north along Renmin Road to the intersection of Renmin Road and Ruichang Road, and entering Nanling Station. The TBM tunnel is a standard single-hole single-line circular section. The interval plane line consists of a linear section, two circular curves, and relief curves with radii of 400 m and 800 m, respectively, with a line spacing of 14-16m, soil thickness of 28-36 m, and a line of 21%; six buildings in this section were simulated, numbered 1-6. The plane positions of the new tunnel and building group are shown in Figure 1.

2.2. Numerical calculation model and the analysis method

1) Model Establishment

Four span x 2 span x 4 layer frame structure, 2 span in tunnel axis direction, 4 span per 6.5m. The foundation is 4.2 m, the foundation for the cross bar is 6.5 m high. Beams, columns, and floors were made of reinforced concrete. The beam section size was 0.3 m x 0.5 m; the column section size was 0.4 m x 0.4 m; the floor thickness was 0.12 m. According to the TBM construction characteristics of Qingdao Metro, the TBM construction parameters and material parameters were: tunnel buried depths of 20 m, 6 m; concrete sheet thickness of 0.3 m, 0.15 m. The soil layer was homogeneous medium weathered granite. The physical and mechanical parameters are shown in Table 1; the three-dimensional numerical model of one tunnel foundation building is shown in Figure 1.

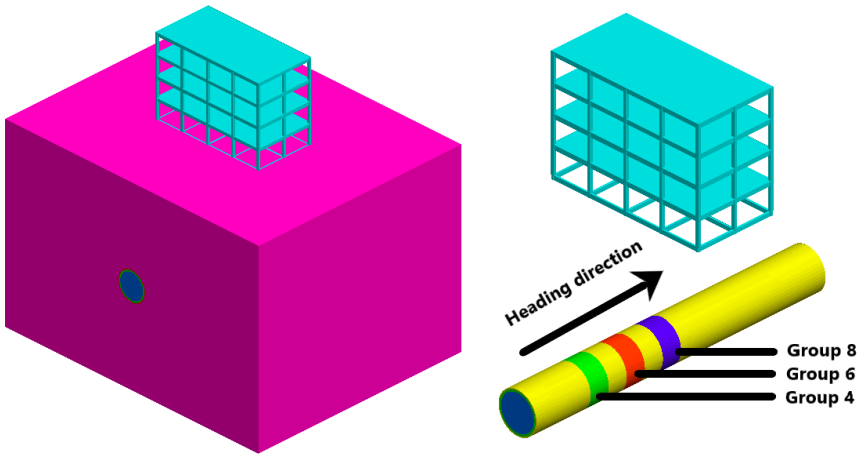

Figure 1. Model of tunnel and frame structure.

Table 1. Material parameters.

Material Name	Density (kg/m)³)	Poisson ratio	Elastic modulus (MPa)	C (kPa)	Φ(°)
Plain fill fill	2000	0.35	37	11	30
Moderately weathered granite	2750	0.3	5000	3000	45
C50 Tube	2500	0.21	20000	/	/
Grouting layer	2100	0.23	1000	/	/

Beams, plates, and columns	2400	0.21	20000	/	/

The calculated model range and boundary conditions: model dimensions: 60 m (x-direction), 48 m (y-direction), 40 m (z-direction). Displacement boundary conditions: horizontal displacement was limited on the sides; the upper and lower surfaces of the model had free boundaries. The Drucker-Prager soil strength criterion was used, with a hexahedral solid unit, frame beam, column floor, and tunnel segments. The soil formation used the Moore Oullen model. The pressure was 0.3 MPa, without the friction of the TBM and surrounding soil.

Simulation calculation process

The construction process for a complex TBM tunnel was simplified to palm surface excavation, transmission of soil slag, installation of pipe sheet structure, and gap grouting between the pipe sheet and stratum. After the excavation of the palm surface, the installation and exchange of the structure, and completion of the structure, there was a gap between the assembled structure and the formation. The purpose was to build a bridge between the formation and the structure; the surrounding rock and the structure could be combined. The surrounding rock on the outer wall of the tunnel squeezed into the reserved gap; as the tunnel passed, the disturbed surrounding rock was consolidated, resulting in deformation of the surrounding rock near the tunnel and redistribution of the formation. To reduce deformation, grout was pressed through the grouting hole through the pipe space.

The numerical analysis process is described as follows:

① The boundary condition model restricts the normal displacement; soil at the top of the model is the free surface.

② The initial ground stress setting considers vertical acceleration due to gravity (9.8 m/s2). The calculation accuracy is 0.0001; tunnel excavation simulation is conducted after the self-weight stress calculation.

③ Excavation method: the shield tunneling method inlet ruler is 1.5 m. Due to the long length and the hard lower rock layer, the excavation lining is laid once every 3 m to save calculation time. In this simulation, the left tunnel was excavated before the right tunnel.

④ The pipe sheet concrete strength grade is C50; the pipe sheet thickness is 300 mm; the post-wall grouting concrete thickness is 150 mm.

3. Analysis of numerical calculation results

The stress in the structure is related to the location of the structure. As the pipe piece is an assembled structure, the force of the pipe piece changes with the excavation. The piece is 1.5 m long; one ring and two rings are one group. Pipe pieces at different positions were selected for stress analysis of the structure. The eighth group of segments (21-24 m directly below the building), the sixth group of segments (15-18 m directly below the building), and the fourth group of segments (9-12 m in front of the building) were selected for analysis. The output results were displayed using curve drawings.

3.1. Case 1: Structural stress and deformation of Group 4 of pipe piece

The stress and deformation of a group of segments located at an excavation diameter D (d = 6 m) under the building structure were considered. The segments were located 6 m in front of the building; the seventh and eighth ring segments were excavated. When the tunnel was excavated to the front of Group 4, the segment structure of Group 4 was not stressed. Thus, in Group 4, the structure works after excavation to the fourth loading step. Figures 2 and 4 show the stress and displacement nephograms of the segment after completion of tunnel excavation; Figures 3 and 5 show the deformation and displacement curves of the vault, arch bottom, and arch waist of the segment with tunnel excavation.

Preprints (www.preprints.org) | NOT PEER-REVIEWED | Posted: 19 July 2023 doi:10.20944/preprints202307.1312.v1

Figure 2 shows the stress nephograms of Group 4 after completion of tunnel excavation. In Figure 2a, the stress of the segments in the x-direction is negative, and the maximum stress reaches 0.181 MPa at the inclined 45°on the left and right sides of the arch bottom. In Figure 2b, the stress in the y-direction is also negative, and the maximum stress value reaches 0.14 MPa at the arch waist on both sides. In Figure 2c, the stress in the z-direction is negative, and the maximum stress value reaches 0.57 MPa in the arch waist on both sides of the segment.

Figure 3 shows the stress curves of the vault, arch waist, and arch bottom outside the segment during tunnel excavation. The data collected after 9 m of excavation are stress data outside the segment. In Figure 3a, the absolute value of the stress in the x-direction is the largest; the stress just after the segment is laid reaches 67 kPa; the stress in the y- and z-directions is almost the same. In Figure 3b, the stress in the z-direction of the arch waist is the largest, followed by the stress in the y-direction and the x-direction. The stress at the arch waist increases slowly with excavation. In Figure 3c, the z-direction arch bottom stress was the largest; the stress differences in the three directions were not large, and were small with increasing excavation.

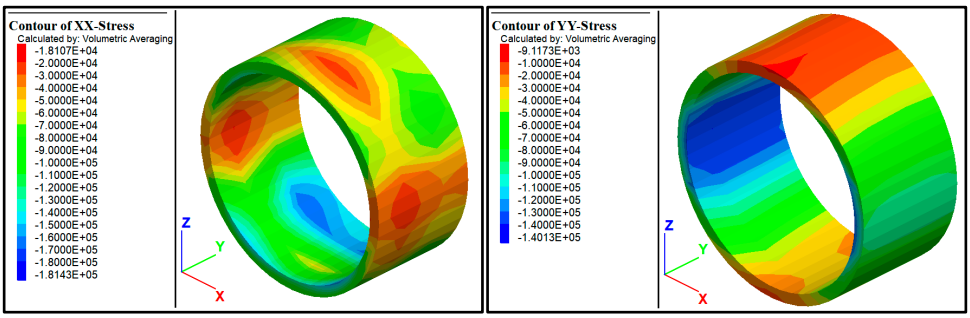

(a) XX stress (b) YY stress

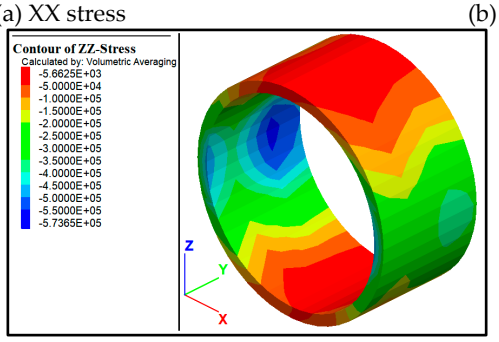

(c) ZZ stress

Figure 2. Internal force diagrams of fourth segment.

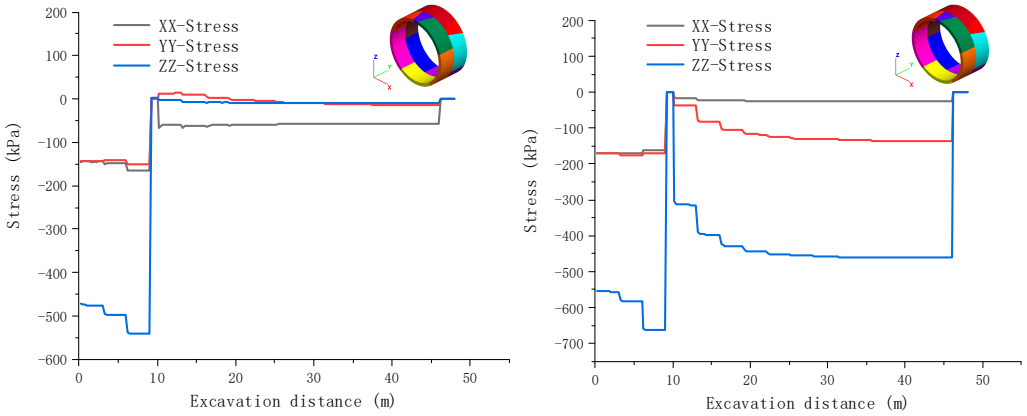

(a) Segment top (b) Segment waist

Preprints (www.preprints.org) | NOT PEER-REVIEWED | Posted: 19 July 2023 doi:10.20944/preprints202307.1312.v1

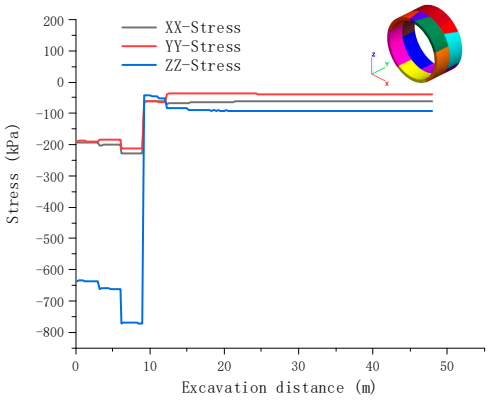

(c) Segment bottom

Figure 3. Stress curves of segment at different positions.

Figure 4 shows the displacement nephograms of the fourth group of segments after completion of tunnel excavation. In Figure 4a, the displacement of segments in the x-direction reaches the maximum at the two sides of the arch waist, and the maximum displacement reaches 0.0197 mm. In Figure 4b, the displacement in the y-direction is negative (in the direction of tunnel excavation). The maximum stress reaches 0.0375 mm at the edge of the segment ring. In Figure 2c, the displacement of the vault and the arch bottom is the largest in the z-direction, and the maximum displacement reaches 0.2 mm; the vertical displacement is the largest in all parts of the segment.

Figure 5 shows the displacement curves of the segment vault, the arch waist, and the outside of the arch bottom during tunnel excavation. The data collected after 9 m of tunnel excavation are segment displacement data. In Figure 5a, the displacement value in the z-direction is the largest in the vault. After laying the segments, the displacement value increases rapidly, reaching 0.035 mm when the excavation reaches 12 m, and increasing to more than 0.06 mm with continued excavation. The displacement values in the x- and y-directions are relatively similar. In Figure 5b, the displacement values for the arch waist are relatively similar in the three directions, and increase with excavation. In Figure 5c, the z-direction displacement value of the arch bottom is the largest, and increases rapidly with excavation; the maximum value reaches 0.45 mm. There is little difference between the x-direction and y-direction displacement values, which are small with increasing excavation.

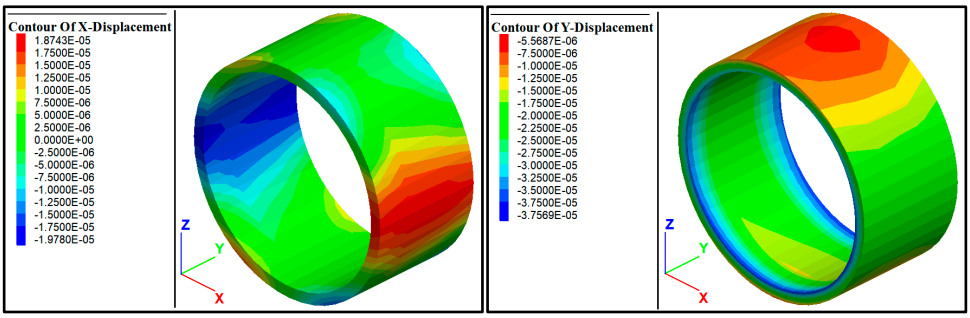

(a) X displacement (b) Y displacement

Preprints (www.preprints.org) | NOT PEER-REVIEWED | Posted: 19 July 2023 doi:10.20944/preprints202307.1312.v1

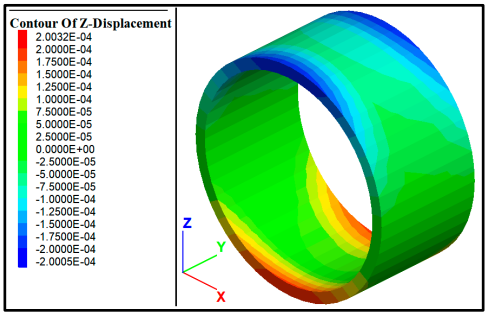

(c) Z displacement

Figure 4. Segment displacement diagrams for fourth group.

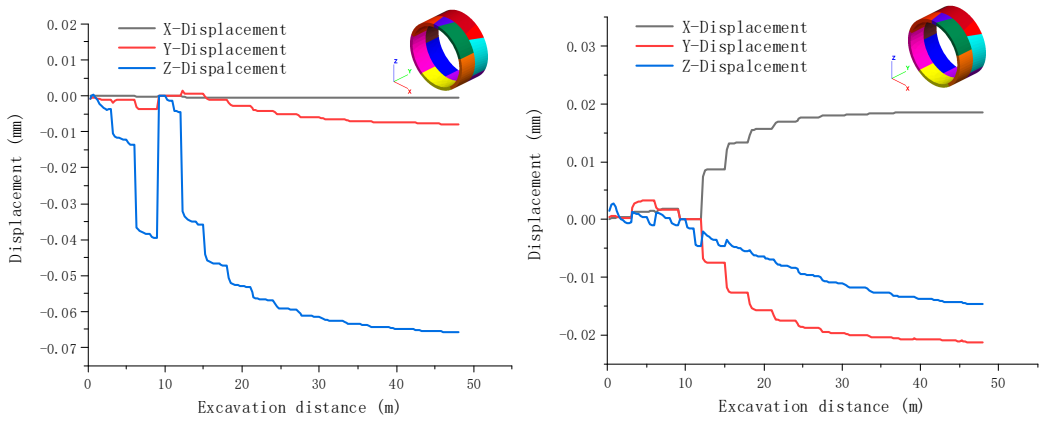

(a) Segment top (b) Segment waist

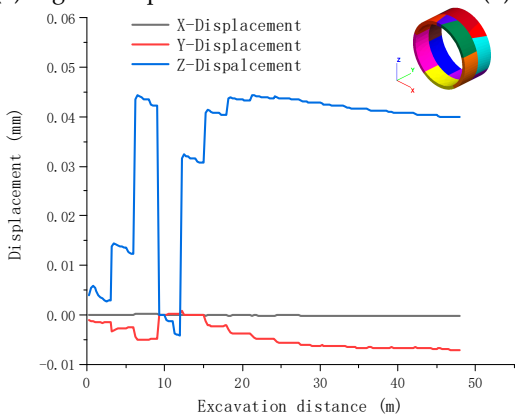

(c) Segment bottom

Figure 5. Displacement curves of segment at different positions.

3.2. Case 2: Structural stress and deformation of Group 6 of pipe piece

A group of segments 3 m to 0 m below the building structure was excavated (7th and 8th ring segment structures). When the tunnel was excavated to the front of Group 6, the segment structure of Group 6 was not stressed. In Group 6, the structure works after excavation to the sixth loading step. Figures 6 and 8 show the stress and displacement nephograms of the segment after completion of tunnel excavation. Figures 7 and 9 show the stress and displacement curves of the vault, arch bottom, and arch waist of the segment with tunnel excavation.

Figure 6 shows the stress nephograms of the sixth group of segments after completion of tunnel excavation. In Figure 6a, the stress of segments in the x-direction is negative, and the maximum stress value reaches 0.182 MPa at the inclined 45°on the left and right sides of the arch bottom. In Figure 6b, the stress in the y-direction is also negative, and the maximum stress value reaches 0.138 MPa at

Preprints (www.preprints.org) | NOT PEER-REVIEWED | Posted: 19 July 2023 doi:10.20944/preprints202307.1312.v1

the arch waist on both sides. In Figure 6c, the stress in the z-direction is negative, and the maximum stress value reaches 0.589 MPa in the arch waist on both sides of the segment.

Figure 7 shows the stress curves of the vault, arch waist, and arch bottom outside the segment during tunnel excavation. The data collected after 15 m of tunnel excavation are the stress data outside the segment. In Figure 7a, the absolute value of the stress in the x-direction is the largest, and the stress value just after the segment is laid reaches 19 kPa; the stress in the y- and z-directions is similar. In Figure 7b, the arch waist stress changes little with excavation, and is maintained at 5–30 kPa. In Figure 7c, the stresses in the x-, y-, and z-directions of the arch bottom are almost the same, and are maintained at 0–10 kPa.

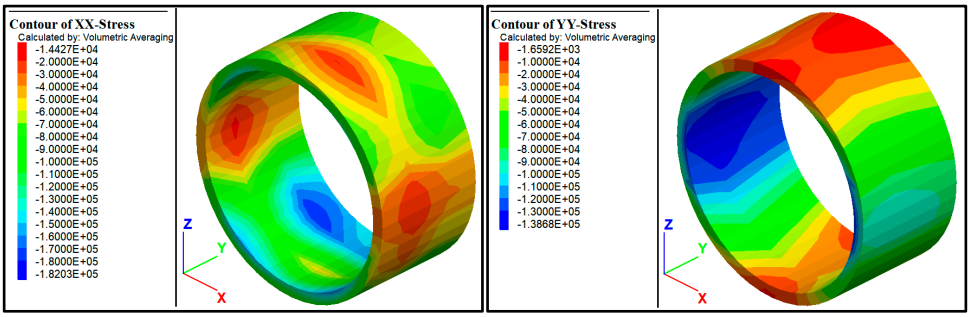

(a) XX stress (b) YY stress

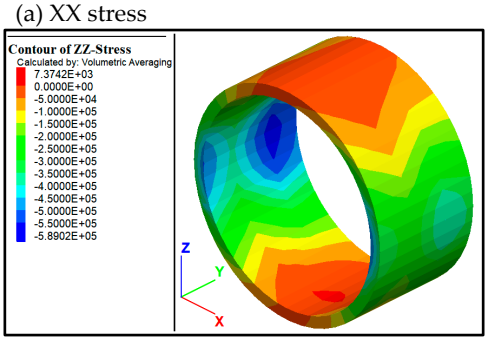

(c) ZZ stress

Figure 6. Internal force diagrams of sixth segment.

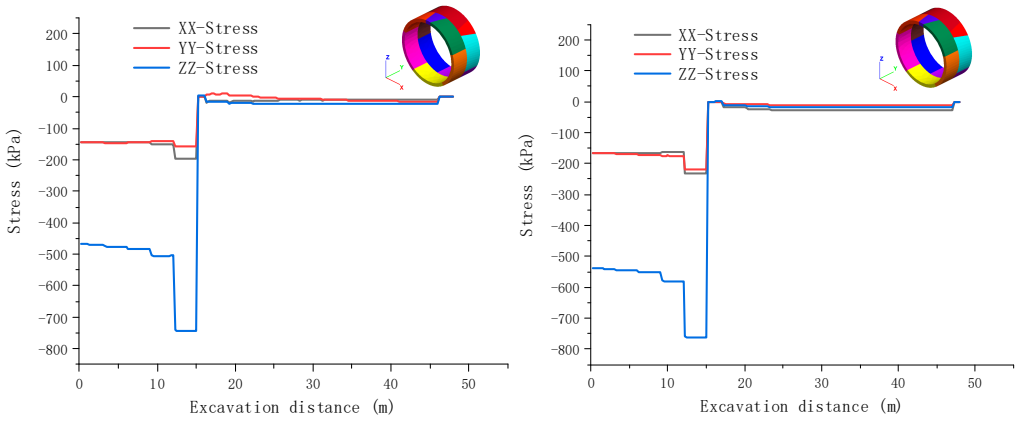

(a) Segment top (b) Segment waist

Preprints (www.preprints.org) | NOT PEER-REVIEWED | Posted: 19 July 2023 doi:10.20944/preprints202307.1312.v1

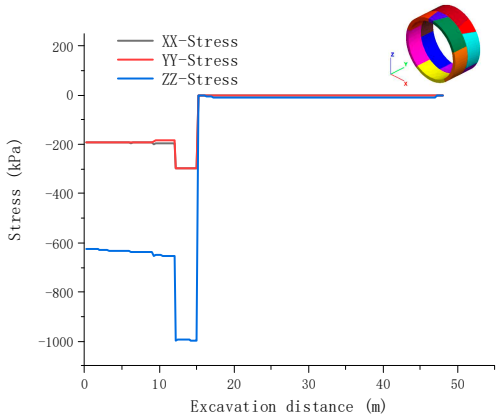

(c) Segment bottom

Figure 7. Stress curves of segment at different positions.

Figure 8 shows the displacement nephograms of the sixth segment after completion of tunnel excavation. In Figure 8a, the displacement of the segment in the x-direction reaches the maximum at the arch waist of both sides; the maximum displacement reaches 0.0192 mm. In Figure 8b, the displacement in the y-direction is negative (in the direction of tunnel excavation). The maximum stress value reaches 0.0369 mm at the edge of the segment ring. In Figure 8c, the displacement of the vault and arch bottom is the largest in the z-direction; the maximum displacement reaches 0.2 mm, and the vertical displacement is the largest in all parts of the segment.

Figure 9 shows the displacement curves of the segment vault, the arch waist, and the outside of the arch bottom during tunnel excavation. The data collected after 15 m of tunnel excavation are the displacement data of the segment. In Figure 9a, the displacement value in the z-direction is the largest in the vault displacement. After laying the segments, the displacement value increases rapidly, reaching 0.035 mm when the excavation reaches 18 m, and increasing to more than 0.06 mm as the excavation continues. The displacement values in the x- and y-directions are relatively similar. In Figure 9b, the displacement values for the arch waist in three directions are relatively similar. The displacement in the x- and y-directions reaches 0.02 mm, and the displacement in the z-direction reaches 0.13 mm; the displacement at the arch waist increases with excavation. In Figure 9c, the z-direction displacement of the arch bottom is the largest, and increases rapidly with excavation; the maximum value reaches 0.47 mm. There is little difference between the x- and y-direction displacement values, which are small with increasing excavation.

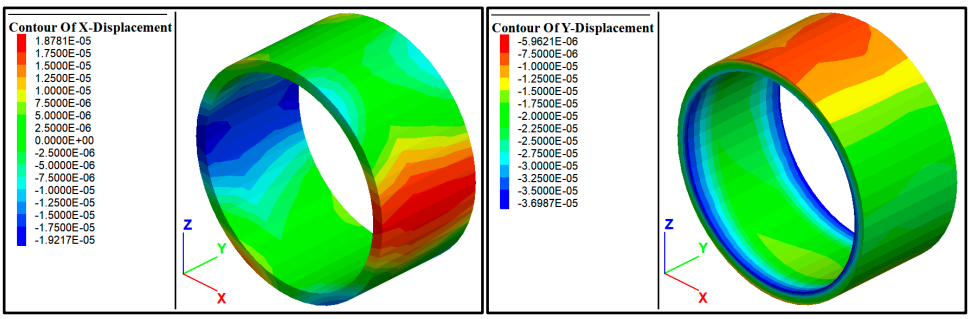

(a) X displacement (b) Y displacement

Preprints (www.preprints.org) | NOT PEER-REVIEWED | Posted: 19 July 2023 doi:10.20944/preprints202307.1312.v1

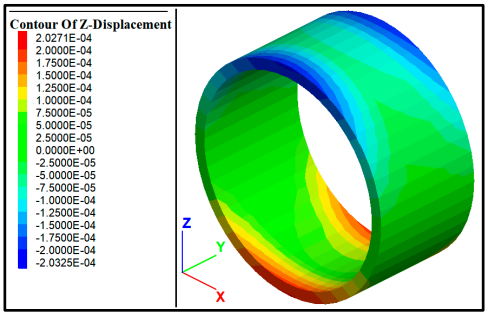

(c) Z displacement

Figure 8. Segment displacement diagrams for sixth group.

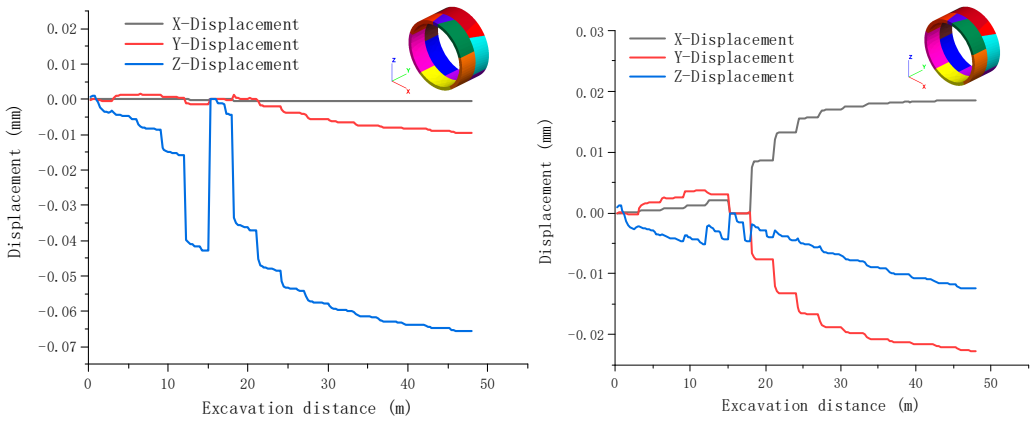

(a) Segment top

(b) Segment waist

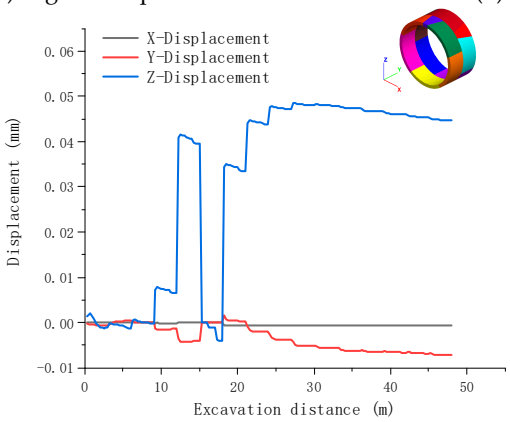

(c) Segment bottom

Figure 9. Stress curves of segment at different positions.

3.3. Case 3: Structural stress and deformation of Group 8 of pipe piece

A group of segments directly below the building structure was excavated (15th and 16th ring segments). When the tunnel was excavated to the front of Group 8, the segment structure of Group 8 was not stressed. In Group 8, the structure worked after excavation to the eighth loading step. Figures 10 and 12 show the stress and displacement nephograms of the segment after completion of tunnel excavation. Figures 11 and 13 show the stress and displacement curves of the vault, arch bottom, and arch waist of the segment with tunnel excavation.

Figure 10 shows the stress nephograms of the 8th segment after completion of tunnel excavation. In Figure 10a, the stress of the segment in the x-direction is negative, and the maximum stress value reaches 0.221 MPa; the position is inclined 45°on the left and right sides of the arch bottom. In Figure 10b, the stress in the y-direction is also negative, and the maximum stress value reaches 0.137 MPa at the arch waist on both sides. In Figure 10c, the stress in the z-direction is negative; the maximum

Preprints (www.preprints.org) | NOT PEER-REVIEWED | Posted: 19 July 2023 doi:10.20944/preprints202307.1312.v1

stress value reaches 0.64 MPa, and the position is concentrated in the arch waist on both sides of the segment.

Figure 11 shows the stress curves of the vault, arch waist, and arch bottom outside the segment during tunnel excavation. The data collected after 21 m of tunnel excavation are the stress data outside the segment. In Figure 11a, the absolute value of the stress in the z-direction is the largest; the stress value just after the segment is laid reaches 40 kPa, and the stress difference in the x- and y-directions is small, approximately 25 kPa. In Figure 11b, the arch waist stress changes little with excavation, and is maintained at 5–30 kPa. In Figure 11c, the stresses in the x-, y-, and z-directions of the arch bottom are almost the same, and are maintained at 0–12 kPa.

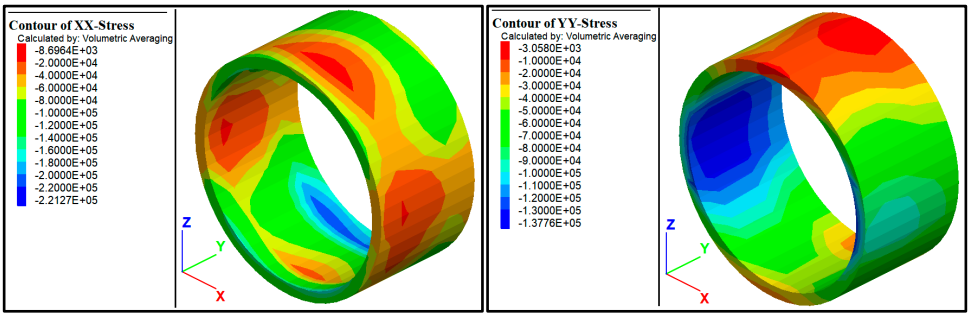

(a) XX stress (b) YY stress

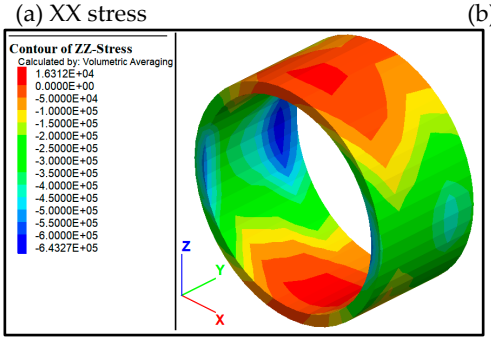

(c) ZZ stress

Figure 10. Internal force diagrams of eighth segment.

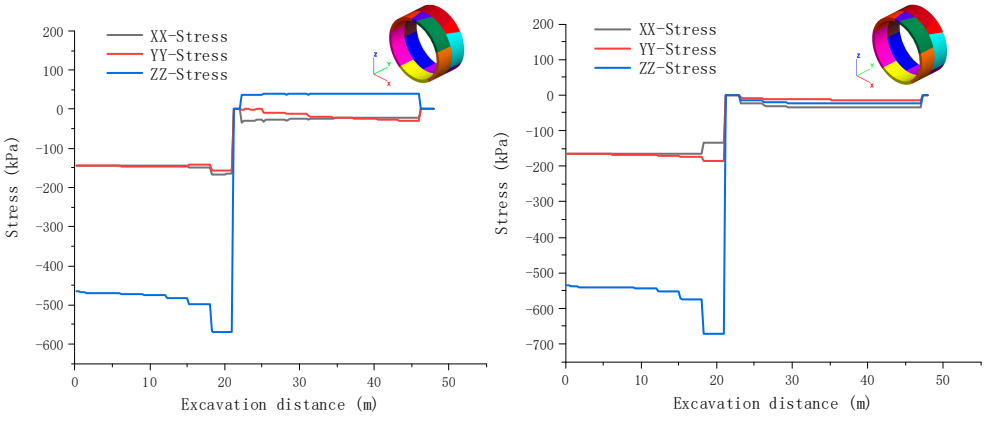

(a) Segment top (b) Segment waist

Preprints (www.preprints.org) | NOT PEER-REVIEWED | Posted: 19 July 2023 doi:10.20944/preprints202307.1312.v1

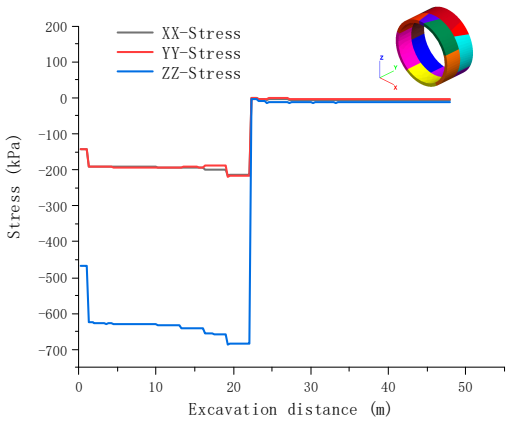

(c) Segment bottom

Figure 11. Stress curve of segment at different positions.

Figure 12 shows the displacement nephograms of the 8th segment after completion of tunnel excavation. In Figure 12a, the displacement of the segment in the x-direction reaches the maximum at the arch waist on both sides; the maximum displacement reaches 0.0208 mm. In Figure 12b, the displacement in the y-direction is negative (in the direction of tunnel excavation). The maximum stress value reaches 0.0389 mm at the edge of the segment ring. In Figure 12c, the displacement of the vault and arch bottom in the z-direction is the largest; the maximum displacement reaches 0.2 mm. The vertical displacement is the largest in all parts of the segment.

Figure 13 shows the displacement curves of the segment vault, arch waist, and the outside of the arch bottom during tunnel excavation. The data collected after 21 m of tunnel excavation are the segment displacement data. In Figure 13a, the displacement in the z- direction is the largest in the arch crown. After laying the segments, the displacement value increases rapidly, reaching 0.032 mm when the excavation reaches 24 m, and increasing to approximately 0.06 mm with excavation. In Figure 13b, the displacement values of the arch waist in three directions are relatively similar; the displacements in the x- and y-directions reach 0.02 mm and the displacement in the z-direction reaches 0.12 mm. The displacement at the arch waist increases with excavation. In Figure 13c, the z-direction displacement of the arch bottom is the largest; it increases rapidly with excavation, and the maximum value reaches 0.41 mm. The displacement in the x-direction is almost unchanged; the displacement in the y-direction increases to 0.01 mm.

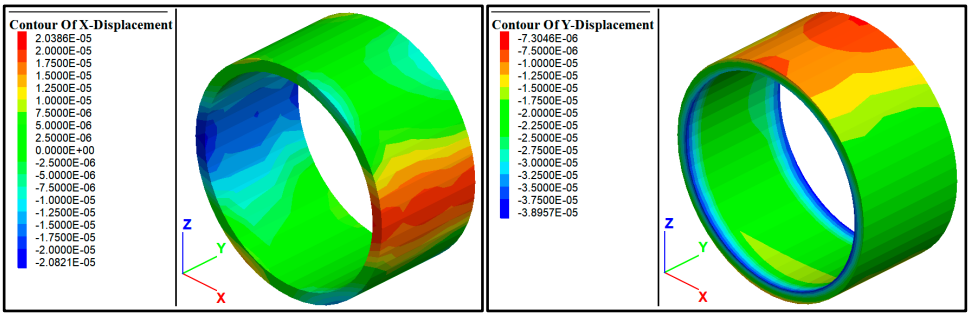

(a) X displacement (b) Y displacement

Preprints (www.preprints.org) | NOT PEER-REVIEWED | Posted: 19 July 2023 doi:10.20944/preprints202307.1312.v1

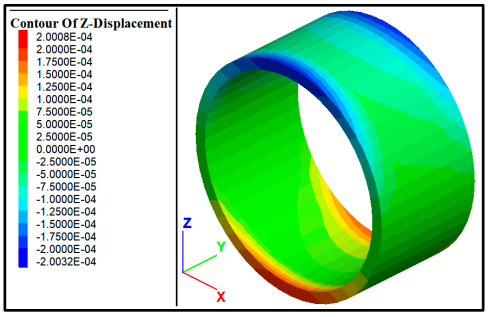

(c) Z displacement

Figure 12. Segment displacement diagrams of eighth group.

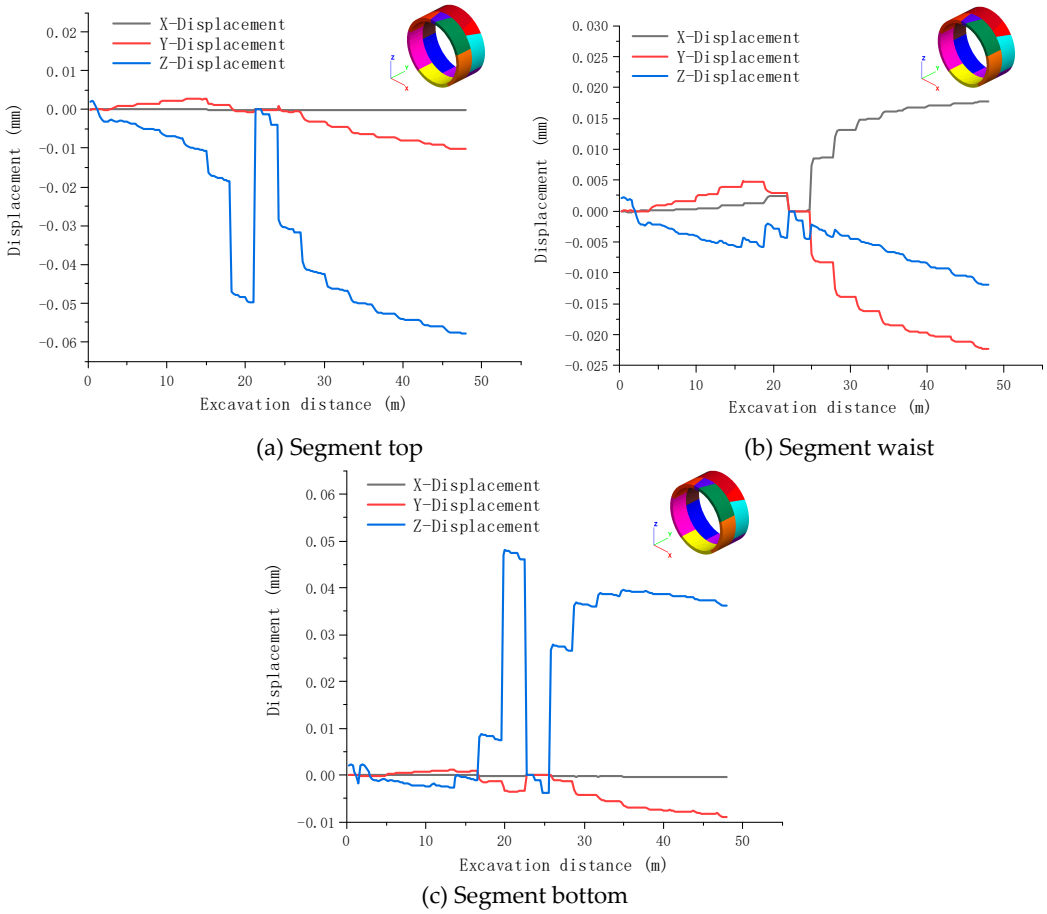

(a) Segment top

(b) Segment waist

(c) Segment bottom

Figure 13. Stress curves of segment at different positions.

4. Surface settlement characteristics analysis in underpass building conditions

Soil displacement is a main cause of damage to surface buildings. Changes in surface subsidence with the advance of the TBM excavation were analyzed. The tunnel was excavated gradually from y = 0 m. Figure 14 shows the surface settlement at distances of 3 m, 12 m, 24 m, 36 m, and 48 m. It is observed that the TBM excavation caused the ground in front of the excavation surface to rise, and the ground behind the excavation surface to sink. With advancing excavation, settlement grooves gradually formed. After the excavation reached 3 m, it had a significant influence on the settlement only within a range of 1.5 times the diameter of the tunnel. The maximum settlement value of the tunnel top was 0.26 mm, with a weak effect on the bottom of the building. After excavation to 12 m, the area affected by settlement had reached the side of the building, with the risk of uneven settlement of the building and the building inclining. When the excavation reached 24 m, the settlement covered almost the entire building area. After 36 m of excavation, the area affected by

Preprints (www.preprints.org) | NOT PEER-REVIEWED | Posted: 19 July 2023 doi:10.20944/preprints202307.1312.v1

settlement completely surrounded the building. At this time, the influence area was distributed in a U-shaped contour. A greater settlement effect on the inner side attachment produced a smaller effect on the outer side; driving the tunnel vertically allowed the building to be added.

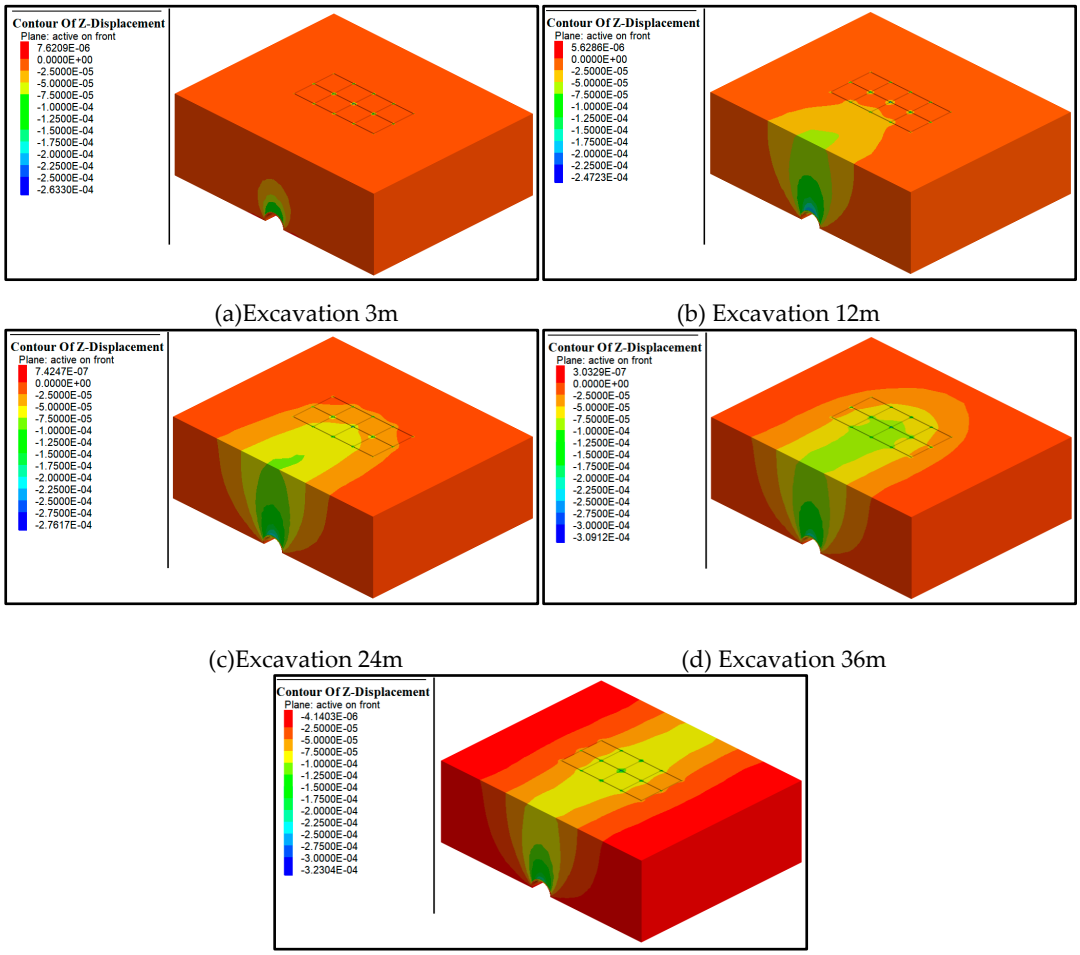

(a)Excavation 3m (b) Excavation 12m

(c)Excavation 24m (d) Excavation 36m

(e) Excavation 48m

Figure 14. Contour maps of vertical ground displacement.

5. Conclusions

Through simulation analysis of the underpass building, it is concluded that:

(1) The stress and deformation of the segments are different at different positions. The horizontal and vertical stress and displacement of the segments in front of the building are significantly affected by the building. When the segment was not in the area below the horizontal plane of the building, the vertical stress of the segment was significantly greater than the two stresses in the horizontal direction.

(2) The vertical displacement of the vault and arch bottom were the largest; the influence of vertical accessories was stronger for segments closer to the building. The horizontal displacement at the vault was small, whereas the horizontal displacement along the tunnel axis was approximately one-sixth of the vertical displacement. The horizontal displacement at the arch waist was similar; the vertical displacement was approximately one-half of the horizontal displacement. The action of the arch bottom on the arch crown was similar, but the displacement was in the opposite direction. The horizontal displacement along the axial direction of the segment was approximately one-fifth of the vertical displacement.

(3) When the tunnel was excavated to approximately the tunnel diameter in front of the building, the building was affected by the influence area. When the surrounding rock was unstable, there was a possibility of collapse of the excavation surface or subsidence of the ground surface, possibly leading to the building inclining, cracking, or settling unevenly. The effects of surface settlement caused by TBM construction are complex, and difficult to accurately calculate and predict. Thus, real-time monitoring and control must be implemented during TBM construction to understand land subsidence information at all times, allowing sufficient time to take effective measures to control subsidence and reduce losses.

Acknowledgements: This work was supported by the National Natural Science Foundation of China(52179106).

References

1. LEE Y L.Explicit analysis for the ground-support interaction of a circular tunnel excavation in anisotropic stress fields[J]. Journal of the Chinese Institute of Engineers, 2020, 43(1):13-26.
2. WU K,CUI S S,ZHANG Q J,et al.Mechanical mechanism of new metro tunnel passing under existing metro tunne[J]. Journal of Jiangsu University(Natural Science Edition)2018, 39(5):596-603
3. WU K, ZHANG W, WU H T, et al. Deformation law of a metro tunnel underneath an existing urban road in combination soft/hard Stratum[J].Modern Tunneling Technology2017,54(6):126-135
4. LEI H, YAO H, LIU Y, et al.Failure mode of shield excavation face using transparent soil[J].Japanese Geotechnical Society Special Publication,2020,8(11):455-458.
5. ZHAO C Y, RAOUL Hölter, MARKUS König, et al. A hybrid model for estimation of ground movements due to mechanized tunnel excavation[J].Computer-Aided Civil and Infrastructure Engineering, 2019, 34(7):586-601.
6. ZHANG S K, YAN J, ZHI H, et al.Transverse extent of numerical model for deep buried tunnel excavation[J].Tunnelling and Underground Space Technology, 2019, 84(2):373-380.
7. ZHANG D M, HUANG Z K,LI Z L, et al. Analytical solution for the response of an existing tunnel to a new tunnel excavation underneath[J].Computers and Geotechnics,2019,108(4):197-211.
8. ZUO Z B, HUANG Y L, WU X J,et al. Numerical simulation of influence of excavation on underneath double metro tunnel[J].Journal of Beijing Jiaotong University,2019,43(3):50-56
9. ZHAI W Z, ZHAI Y X, ZHANG D M,et al. Numerical study on shearing performance of seel plate strengthened circumferential joints of segmental tunnel linings[J].Chinese Journal of Geotechnical Engineering2019,41(2)：235-239.
10. ZHANG Z G, ZHANG C P, XI X G. Closed solutions to soil displacements induced by twin-tunnel excavation under different layout patterns[J].Chinese Journal of Geotechnical Engineering, 2019, 41(2):262-271.